INTERNATIONAL JOURNAL FOR NUMERICAL METHODS IN FLUIDS
Int. J. Numer. Meth. Fluids **29**: 811–826 (1999)

NUMERICAL PREDICTION OF TURBULENT BUBBLY TWO-PHASE FLOW IN A ROTATING COMPLICATED DUCT

JING-CHUN WU* AND KIYOSHI MINEMURA

School of Informatics and Sciences, Nagoya University, Nagoya 464-01, Japan

SUMMARY

A fully three-dimensional numerical procedure based on the two-fluid model in a general curvilinear co-ordinate system is proposed for the prediction of developing turbulent bubbly two-phase flow in a rotating complicated duct. A Coriolis-modified turbulence model is extended to two-phase flows to account for the rotational effect on the lateral phase distribution. The governing equations are solved using a finite volume technique with a non-staggered variable arrangement. Comparisons of the predictions with measured pressure and void fractions show good agreement. Copyright © 1999 John Wiley & Sons, Ltd.

KEY WORDS: phase distribution; turbulence model; two-fluid model; finite volume

1. INTRODUCTION

In view of recent emphases on the safety analysis of nuclear reactors and increased requirements for the offshore oil field developments, it is imperative to understand the mechanisms of gas–liquid two-phase flow in centrifugal pumps, and to establish numerical methods to accurately predict the flow characteristics. For this purpose, Minemura and Uchiyama [1] performed a three-dimensional computation for the air–water two-phase flow in a centrifugal pump impeller. The flow was solved with a finite element method on the basis of a bubbly flow model. Their predictions reasonably captured the flow trends as observed by experiment [2], but with considerable deviations from the data, due to the neglect of the viscosity. Recently, Clark and Issa [3] employed a model proposed by Gosman *et al.* [4] to predict the three-dimensional turbulent bubbly flow in the same centrifugal pump. Their results, however, still showed remarkable differences with the experimental data. Therefore, the numerical simulation of the two-phase flows should be investigated preliminarily for simpler problems due to the complexity of the rotating impeller passage. With the intention of better understanding flow mechanisms, especially the rotational effects on the two-phase flow behavior, air–water two-phase flow in a rotating square-sectioned duct, chosen as a simple model of an impeller passage, was experimentally investigated by Patel and Runstadler [5] and Minemura *et al.* [6]. The flow was then numerically analyzed by Uchiyama *et al.* [7] using a two-dimensional bubbly flow model with Reynolds stress based on the mixing length theory. In the authors previous studies,

* Correspondence to: School of Informatics and Sciences, Nagoya University, Nagoya 464-01, Japan.

CCC 0271–2091/99/070811–16$17.50

Received December 1997
Revised March 1998

three-dimensional numerical predictions were performed for the same duct based on the two-fluid model in a Cartesian co-ordinate system [8], and effects of turbulence on the phase distribution were investigated by using several kinds of turbulence models [9]. Although these computations reasonably predicted the flow trends, the simplification of the computational domain probably contributed greatly to the considerable deviations of the predictions from the measurement.

For the bubbly two-phase flows, turbulence modeling is the key to accurately predicting the phase distribution. In recent years, some advances have been made in modeling turbulence based on the two-fluid model [10–13]. However, most of the numerical analyses have been concerned only with fully developed flows in stationary circular ducts. And to date, there have been few works on two-phase flow in a rotating non-circular duct despite its importance in practical applications. On the other hand, almost all the existing numerical simulations are confined to a Cartesian co-ordinate system and predictions for the two-phase flow in complex geometries are virtually limited. It is, therefore, the objective of this study to advance the state-of-the-art in rotational and multidimensional two-phase flows in arbitrary geometries. A fully three-dimensional numerical procedure based on the two-fluid model in a general curvilinear co-ordinate system is proposed in this paper. Turbulence is modeled using a Coriolis-modified turbulence model [14] to account for the rotational effects. A finite volume technique is employed for the solution of the governing equations, with a non-staggered variable arrangement. In order to avoid decoupling of the velocity and pressure fields, the pressure-weighted interpolation method (PWIM) proposed by Rhie and Chow [15] and then improved by Majumdar [16], is used. A numerical procedure based on the inter-phase slip algorithm (IPSA) proposed by Spalding [17] is developed in this paper. The method is applied to the developing turbulent bubbly two-phase flow in a rotating complicated duct, experimentally studied by Minemura *et al.* [6], which consists of a square-sectioned duct with both ends connected to a circular pipe through a bend. The results obtained herein show fair agreement with the limited data available on this rotating duct.

2. MATHEMATICAL MODELS

2.1. Two-fluid model

For isothermal and incompressible gas–liquid flow in a rotating Cartesian co-ordinate system, the equations of continuity and momentum based on the two-fluid model can be written as:

$$\frac{\partial \alpha_k \rho_k}{\partial t} + \nabla \cdot (\alpha_k \rho_k \boldsymbol{u}_k) = 0 \quad (k = \mathrm{g}, \mathrm{l}), \tag{1}$$

$$\frac{\partial (\alpha_k \rho_k \boldsymbol{u}_k)}{\partial t} + \nabla \cdot (\alpha_k \rho_k \boldsymbol{u}_k \boldsymbol{u}_k)$$
$$= -\alpha_k \nabla p_k + \nabla \cdot \alpha_k \tau_k + \nabla \cdot \alpha_k \tau_k^t + \alpha_k \rho_k \mathbf{g} - \alpha_k \rho_k [\boldsymbol{\Omega} \times (\boldsymbol{\Omega} \times \boldsymbol{r}) + 2\boldsymbol{\Omega} \times \boldsymbol{u}_k] + \boldsymbol{M}_k, \tag{2}$$

where the subscript k denotes liquid (l) or gas phase (g).

It is now assumed that the surface tensions are negligible, which implies that the pressure within each phase is the same, i.e. $p_k = p$. Under this assumption, the interfacial force $\boldsymbol{M}_k$ is reduced to $\boldsymbol{M}_\mathrm{l} = -\boldsymbol{M}_\mathrm{g}$. The interfacial force can be decomposed into several terms such as drag force $\boldsymbol{M}^\mathrm{d}$, virtual mass force $\boldsymbol{M}^\mathrm{vm}$ and lift force $\boldsymbol{M}^\mathrm{l}$. For the gas phase, we have:

$$\boldsymbol{M}_{\mathrm{g}} = \boldsymbol{M}_{\mathrm{g}}^{\mathrm{d}} + \boldsymbol{M}_{\mathrm{g}}^{\mathrm{vm}} + \boldsymbol{M}_{\mathrm{g}}^{\mathrm{l}}. \tag{3}$$

The interfacial drag force for spherical bubbles with the diameter of D_{b} is modeled as:

$$\boldsymbol{M}_{\mathrm{g}}^{\mathrm{d}} = F_{\mathrm{d}}(\boldsymbol{u}_{\mathrm{l}} - \boldsymbol{u}_{\mathrm{g}}) \tag{4}$$

and F_{d} is given by:

$$F_{\mathrm{d}} = (3\alpha_{\mathrm{g}}/4D_{\mathrm{b}})\rho_{\mathrm{l}} C_{\mathrm{D}} |\boldsymbol{u}_{\mathrm{l}} - \boldsymbol{u}_{\mathrm{g}}|. \tag{5}$$

Here, the drag coefficient C_{D} is obtained via the empirical correlations proposed by Ishii and Zuber [18]:

$$C_{\mathrm{D}} = (24/Re_{\mathrm{b}})(1 + 0.1Re_{\mathrm{b}}^{0.75}), \tag{6}$$

where Re_{b} is the bubble Reynolds number.

Drew and Lahey [19] have derived theoretical models for the lift and virtual mass forces as expressed by:

$$\boldsymbol{M}_{\mathrm{g}}^{\mathrm{l}} = C_{\mathrm{L}}\alpha_{\mathrm{g}}\rho_{\mathrm{l}}(\boldsymbol{u}_{\mathrm{l}} - \boldsymbol{u}_{\mathrm{g}}) \times (\nabla \times \boldsymbol{u}_{\mathrm{l}}), \tag{7}$$

$$\boldsymbol{M}_{\mathrm{g}}^{\mathrm{vm}} = C_{\mathrm{vm}}\alpha_{\mathrm{g}}\rho_{\mathrm{l}}\left(\frac{D_{\mathrm{l}}\boldsymbol{u}_{\mathrm{l}}}{Dt} - \frac{D_{\mathrm{g}}\boldsymbol{u}_{\mathrm{g}}}{Dt}\right), \tag{8}$$

where C_{L} is the lift coefficient, and C_{vm} the virtual mass coefficient. According to Drew and Lahey [19], the combination of virtual mass and lift forces is objective only if $C_{\mathrm{L}} = C_{\mathrm{vm}}$. In this study, the typical value of 0.5 is taken for the both coefficients.

2.2. Turbulence model

The standard k–ϵ model was first employed by Lee *et al.* [10] for the bubbly flow in vertical pipes. Lopez de Bertodano and his co-workers [11] applied a τ–ϵ model to the bubbly pipe flows to account for the anisotropy of turbulence, which was shown to have a substantial effect on the phase distribution by their studies. They further adapted the k–ϵ model [12] to the bubbly flows by assuming that the shear-induced and bubble-induced turbulence is linearly superposed. The assumption of linear superposition is based on the experimental evidence of Lance and Bataille [20]. However, many other experimental results [21,22] imply otherwise. Recently, Gosman *et al.* [4] and Issa and Oliveira [23] have extended the single-phase k–ϵ model to a formation to account for the phase fraction fluctuations. Although all these models have been claimed to yield results in good agreement with Serizawa's [21] or Wang's [24] data for the upward and downward bubbly flows in a vertical pipe, the authors' experience in the rotating duct [9] has shown that they may give quite a different phase distribution. In particular, the sources of turbulence kinetic energy and dissipation related to the phase fraction fluctuations seem to excessively underpredict the void fraction. A previous study [9] also shows that the Reynolds stress anisotropies have inconsiderable effects on the pressure, axial and secondary flows, except for some effects on the void fractions. Therefore, the single-phase standard k–ϵ model with rotational modification, as proposed by Howard [14], is extended to the two-phase flow in this study. For the bubbly two-phase flow, the Reynolds stresses of the gas-phase are small in comparison with those of the liquid-phase, so they can be neglected. The Coriolis-modified turbulence model for liquid-phase takes the form (for convenience the subscript l is omitted):

$$\frac{\partial}{\partial t}(\alpha\rho k) + \frac{\partial}{\partial x_i}(\alpha\rho u_i k) = \frac{\partial}{\partial x_i}\left[\alpha\left(\mu + \frac{\mu^t}{\sigma_k}\right)\frac{\partial k}{\partial x_i}\right] + \alpha G - \alpha\rho\epsilon + \alpha G_{\mathrm{c}}, \tag{9}$$

$$\frac{\partial}{\partial t}(\alpha\rho\epsilon)+\frac{\partial}{\partial x_i}(\alpha\rho u_i\epsilon)=\frac{\partial}{\partial x_i}\left[\alpha\left(\mu+\frac{\mu^t}{\sigma_\epsilon}\right)\frac{\partial\epsilon}{\partial x_i}\right]+C_1\alpha\frac{\epsilon}{k}G-C_2\alpha\rho\frac{\epsilon^2}{k}+\alpha G_c\frac{\epsilon}{k}, \tag{10}$$

where the turbulence kinetic energy generation rate G, is:

$$G=\mu^t\frac{\partial u_i}{\partial x_j}\left(\frac{\partial u_i}{\partial x_j}+\frac{\partial u_j}{\partial x_i}\right) \tag{11}$$

and the turbulent viscosity μ^t is given by:

$$\mu^t=C_\mu\rho k^2/\epsilon. \tag{12}$$

G_c in Equations (9) and (10) is a Coriolis modification proposed by Howard *et al.* [14], it takes the form:

$$G_c=9\Omega\mu^t\frac{\partial u}{\partial y}. \tag{13}$$

The constants in the k–ϵ model are assigned the same values as normally used in single-phase flow: $C_\mu=0.09,\ \sigma_k=1.0,\ \sigma_\epsilon=1.3,\ C_1=1.44,\ C_2=1.92$.

2.3. Transformation of basic equations

The above conservation equations typically can be written in a Cartesian co-ordinate system for the dependent variable ϕ_k ($k=$ g, l) in the following form:

$$\frac{\partial}{\partial t}(\alpha_k\rho_k\phi_k)+\frac{\partial}{\partial x_i}(\alpha_k\rho_k u_{ki}\phi_k)=\frac{\partial}{\partial x_i}\left(\alpha_k\Gamma_k^\phi\frac{\partial\phi_k}{\partial x_i}\right)+S_k^\phi, \tag{14}$$

where Γ_k^ϕ is the effective diffusion coefficient and S_k^ϕ the source term. When general curvilinear co-ordinates ξ_j ($j=1, 2, 3$ for ξ, η, ζ) are introduced, Equation (14) changes according to the general transformation $\xi_j=\xi_j(x, y, z)$. The transformed equation can be expressed as follows (for convenience the subscript k for gas- or liquid-phase is omitted):

$$\frac{\partial}{\partial t}(\alpha\rho\phi J)+\frac{\partial}{\partial\xi_j}(\alpha\rho U_j\phi)=\frac{\partial}{\partial\xi_j}\left(\alpha\Gamma^\phi Jq_{j1}\frac{\partial\phi}{\partial\xi_1}\right)+S^\phi J, \tag{15}$$

where U_j ($j=1, 2, 3$ for U, V, W) are the contravariant velocity components:

$$\begin{bmatrix}U\\V\\W\end{bmatrix}=J\begin{bmatrix}\xi_x&\xi_y&\xi_z\\\eta_x&\eta_y&\eta_z\\\zeta_x&\zeta_y&\zeta_z\end{bmatrix}\begin{bmatrix}u\\v\\w\end{bmatrix}, \tag{16}$$

J is the Jacobian of the transformation:

$$J=\frac{\partial(x, y, z)}{\partial(\xi, \eta, \zeta)}=\begin{bmatrix}x_\xi&y_\xi&z_\xi\\x_\eta&y_\eta&z_\eta\\x_\zeta&y_\zeta&z_\zeta\end{bmatrix} \tag{17}$$

and q_{ij} is defined as

$$q_{ij}=\frac{\partial\xi_i}{\partial x_1}\cdot\frac{\partial\xi_j}{\partial x_1}. \tag{18}$$

3. NUMERICAL ALGORITHM AND CALCULATING CONDITIONS

3.1. Discretization of the transport equations

A finite volume technique is employed for the solution of the governing equations with a non-staggered variable arrangement. In order to stabilize a numerical solution and assure a high numerical accuracy, the second-order upwind scheme as developed by Shyy *et al.* [25] and Peric [26] is implemented in the calculation for the two-fluid model.

After discretizing the governing equations, the linearized conservation equations can be written in the following conventional form:

$$a_p\phi_p = \sum_{\mathrm{nb}} a_{\mathrm{nb}}\phi_{\mathrm{nb}} + S_\phi, \tag{19}$$

where a denotes the convection and diffusion contributions in linearized conservation equations, S_ϕ is the corresponding total source term, and nb represents the neighboring points of P as shown in Figure 1.

The discretized set of equations is solved iteratively and sequentially based on the SIMPLE algorithm for single-phase flows, suitably extended to cater for two-phase flows. At the time level t^{n+1}, it is assumed that velocity components $u_i^{k(n+1)}$ of gas- or liquid-phase can be approximated by $u_i^k{}^*$ in the following form:

$$a_p^k u_i^k{}_p^* = \sum_{\mathrm{nb}} a_{\mathrm{nb}}^k u_i^k{}_{\mathrm{nb}}^* + S_{u_i}^k - \alpha^k(\xi_{x_i} p_\xi^* + \eta_{x_i} p_\eta^* + \zeta_{x_i} p_\zeta^*)J + a_0^k u_{p_i}^{k(n)} \quad (k = \mathrm{g}, \mathrm{l}), \tag{20}$$

where $a_0^k = J(\alpha_k\rho_k + C_{\mathrm{vm}}\alpha_{\mathrm{g}}\rho_{\mathrm{l}})/\delta t$, $a_p^k = \Sigma_{\mathrm{nb}}\, a_{\mathrm{nb}}^k + a_0^k$ and the superscript n denotes old time level.

To satisfy the continuity equations, the velocity components $u_i^{k(n+1)}$ are then assumed to be updated by the following relations:

$$u_i^{k(n+1)} = u_i^k{}^* - \frac{\alpha^k J}{a_p^k}(\xi_{x_i} p'_\xi + \eta_{x_i} p'_\eta + \zeta_{x_i} p'_\zeta), \tag{21}$$

where p' is the pressure correction that is related to the pressure p^{n+1} according to:

$$p^{n+1} = p^* + p'. \tag{22}$$

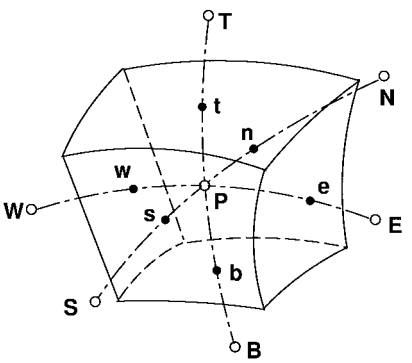

Figure 1. Typical control volume.

Subsequently, the correction forms for the contravariant velocities U_i (U, V, W) are obtained by substituting Equation (21) into Equation (16):

$$U_i^{k(n+1)} = U_i^k * - \frac{\alpha^k J^2}{a_p^k} q_{ij} p'_{\xi_j}. \tag{23}$$

It is noted that the terms $q_{ij}p'_{\xi_j}$ of Equation (23) for $i \neq j$ are negligible if the grid is nearly orthogonal. Neglecting these terms, U_i can be further simplified as:

$$U_i^{k(n+1)} = U_i^k * - B_i^k p'_{\xi_i}, \tag{24}$$

where

$$B_i^k = \frac{\alpha^k J^2}{a_p^k} q_{ii}.$$

3.2. Pressue–velocity coupling

In this study, the pressure correction equation is based on the sum of gas- and liquid-phase continuity equations, each normalized by a reference phase density, as done by Issa and Oliveira [23]. According to Equation (15), the transformed gas- and liquid-phase continuity equations can be written as:

$$\frac{\partial}{\partial t}(\alpha_k \rho_k J) + \frac{\partial}{\partial \xi}(\alpha_k \rho_k U_k) + \frac{\partial}{\partial \eta}(\alpha_k \rho_k V_k) + \frac{\partial}{\partial \zeta}(\alpha_k \rho_k W_k) = 0 \quad (k = \mathrm{g}, \mathrm{l}). \tag{25}$$

Therefore, the sum of gas- and liquid-phase continuity equations can be expressed by:

$$\frac{\partial}{\partial \xi}(\alpha_\mathrm{l} U_\mathrm{l}) + \frac{\partial}{\partial \eta}(\alpha_\mathrm{l} V_\mathrm{l}) + \frac{\partial}{\partial \zeta}(\alpha_\mathrm{l} W_\mathrm{l}) + \frac{\partial}{\partial \xi}(\alpha_\mathrm{g} U_\mathrm{g}) + \frac{\partial}{\partial \eta}(\alpha_\mathrm{g} V_\mathrm{g}) + \frac{\partial}{\partial \zeta}(\alpha_\mathrm{g} W_\mathrm{g}) = 0, \tag{26}$$

where the time derivative terms vanish, since $\alpha_\mathrm{l} + \alpha_\mathrm{g} = 1$ holds at any time.

The pressure correction equation can be obtained by substituting U_i^k from Equation (24) into Equation (26). In order to avoid decoupling of the velocity and pressure fields with the use of non-staggered grids, the PWIM proposed by Rhie and Chow [15] and then improved by Majumdar [16] is used in the present solution procedure to determine the convective velocities. With the introduction of the PWIM, the east cell face contravariant velocity U_e (for convenience, the superscript k for gas- or liquid-phase is omitted) for example, can now be expressed as follows:

$$U_\mathrm{e}^{n+1} = U_\mathrm{e}^* - \overline{B_\mathrm{l}} p'_\xi|_\mathrm{e}, \tag{27}$$

where the overbar indicates linear interpolation, and

$$U_\mathrm{e}^* = \overline{U_\mathrm{e}^*} + (1-\omega)(U_\mathrm{e}^n - \overline{U_\mathrm{e}^n}) + \omega(\overline{B_\mathrm{l} p_\xi^*}|_\mathrm{e} - \overline{B_\mathrm{l} p_\xi^*}|_\mathrm{e}) + \omega\left[\overline{\left(\frac{a_0}{a_p}\right)} U_\mathrm{e}^n - \overline{\left(\frac{a_0}{a_p}\right) U^n}\Big|_\mathrm{e}\right], \tag{28}$$

where ω denotes the underrelaxation factor used for the solution of discretized momentum equations. This expression can give a unique converged solution independent of the underrelaxation factor [16]. The last two terms introduced into the formulation are similar to those given by Issa and Oliveira [23], which also make it give a fully converged solution independent of the time step δt.

Now, with the conception of PWIM, the pressure correction equation can be expressed in the following form:

$$a_p p' = \sum_{\mathrm{nb}} a_{\mathrm{nb}} p'_{\mathrm{nb}} + S_p, \tag{29}$$

where

$$a_{\mathrm{nb}} = a^{\mathrm{l}}_{\mathrm{nb}} + a^{\mathrm{g}}_{\mathrm{nb}} = (\alpha_{\mathrm{l}}\overline{B^{\mathrm{l}}_i} + \alpha_{\mathrm{g}}\overline{B^{\mathrm{g}}_i})\big|_{\mathrm{e,w,n,s,t,b}}, \tag{30}$$

$$S_p = \sum_{k=\mathrm{l,g}} \{(\alpha_k U^*_k)_{\mathrm{e}} - (\alpha_k U^*_k)_{\mathrm{w}} + (\alpha_k V^*_k)_{\mathrm{n}} - (\alpha_k V^*_k)_{\mathrm{s}} + (\alpha_k W^*_k)_{\mathrm{t}} - (\alpha_k W^*_k)_{\mathrm{b}}\}. \tag{31}$$

Here, α_k at the cell face always takes the upwinded values according to the sign of the corresponding cell face contravariant velocities, for example:

$$(\alpha U^*)_{\mathrm{e}} = \alpha_P \max[U^*_{\mathrm{e}}, 0] - \alpha_E \max[-U^*_{\mathrm{e}}, 0]. \tag{32}$$

3.3. Numerical procedure

The above sets of discretized equations for the two-fluid model are solved iteratively and sequentially based on the ISPA proposed by Spalding [17]. The advancement in time is adopted herein by a so-called 'pseudo time marching' technique proposed by Issa and Oliveira [23]. The solution procedure can be summarized as follows:

1. Solve the momentum equations (20) to obtain the liquid- and gas-phase velocities, $u^{\mathrm{l}}_i{}^*$ and $u^{\mathrm{g}}_i{}^*$.
2. Solve the pressure correction equation (29), where the cell face contravariant velocities in S_p are calculated using Equation (28), to obtain the pressure correction p'.
3. The pressure, velocities and contravariant velocities are updated according to Equations (22), (21), (24) and (27) respectively.
4. k and ϵ are solved for using Equation (19).
5. Solve the liquid- and gas-phase continuity equations (25) to obtain the updated phase fractions α_k.
6. The solution will be advanced in time and the iteration process (2)–(5) will be repeated until the convergence is achieved.

3.4. Geometry and boundary conditions

The flow configuration shown in Figure 2 is a rotating complicated duct, where a square-sectioned straight duct (width $D = 32$ mm) is attached to the vertical circular pipe (diameter $D = 32$ mm) by a circular-sectioned 90° bend through a transition section at both ends. The geometry is almost the same as the real configuration of the experimental study by Minemura *et al.* [6]. A detailed description of the geometry and experimental apparatus can be found in [6]. The computational mesh of $114 \times 34 \times 34$ is used in the calculation as representatively shown in Figure 2.

Since the measurements by Minemura *et al.* are primarily confined to the horizontal center plane of the square-sectioned duct, the flow conditions at both the inlet and outlet should be specified. At the inlet, the phase fraction is assumed to be uniform. The axial velocities of both phases are assumed to obey a 1/7-power law distribution. The averaged axial slip velocity $(w_{\mathrm{g}} - w_{\mathrm{l}})$ is specified by a drift flux correlation proposed by Zuber and Findley [28] as in the following:

$$w_{\mathrm{g}} - w_{\mathrm{l}} = \sqrt{2}\,(\sigma g \Delta\rho / \rho_{\mathrm{l}}^2)^{1/4} \alpha_{\mathrm{l}}^n \quad (n = 0.5 \sim 1.0). \tag{33}$$

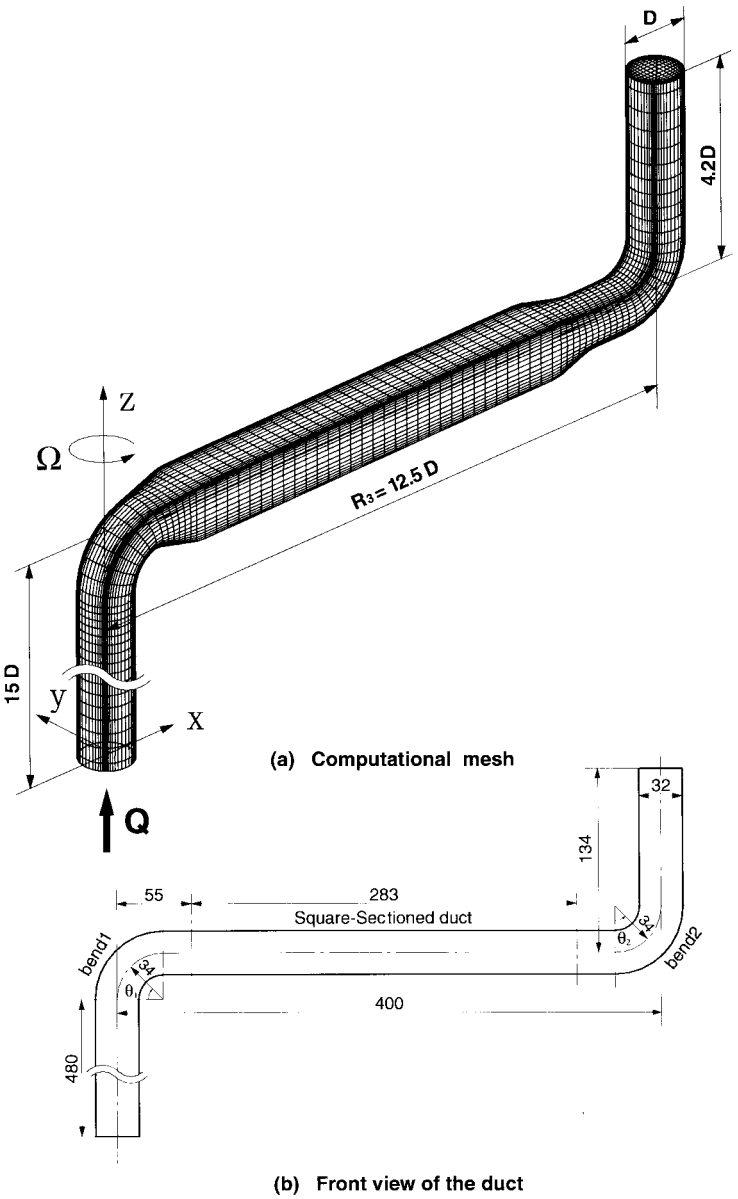

Figure 2. Flow configuration and computational mesh.

At the outlet boundary, zero streamwise gradients are imposed for all variables except pressure for which a linear extrapolation is used. The logarithmic law of the wall has been widely used in single-phase flows. Although there is a deficiency in the performance of the logarithmic law of the wall for the problems involving rotation and curvature, a previous study [29] has shown that the law of the wall can yield fairly good results for the single-phase flow in curved rotating ducts when it is combined with the use of the Coriolis-modified turbulence model as proposed by Howard *et al.* [14]. Various numerical studies have shown that it is also

an effective and reasonable approximation [27] for two-phase flows. Thus, the law of the wall for the solid surfaces is used in this study.

In this work predictions are performed for a Reynolds number ($Re = \rho_l u_b D/\mu_l$) of 25000 and a Rossby number ($Rw = \Omega D/u_b$) of 0.24, with an averaged inlet void fraction of 0.032. The bubble diameter D_b is taken to be 2 mm according to the values of 1–2 mm observed by Minemura *et al.* [6] during their experiments.

4. RESULTS OF SINGLE-PHASE LIQUID FLOW

To evaluate the validity of the present approach, computations are first performed for the single-phase liquid flow with the above Reynolds and Rossby number. The flow evolution through different cross sections is displayed in Figure 3 by the predicted secondary velocity vectors and the corresponding streamwise velocity contours. At the station of $\theta_1 = 60°$ shown in Figure 3(a), the lateral pressure gradient set up by the curvature of the first bend and rotation of the duct, leads to the formation of a pair of asymmetric streamwise vortices. Such

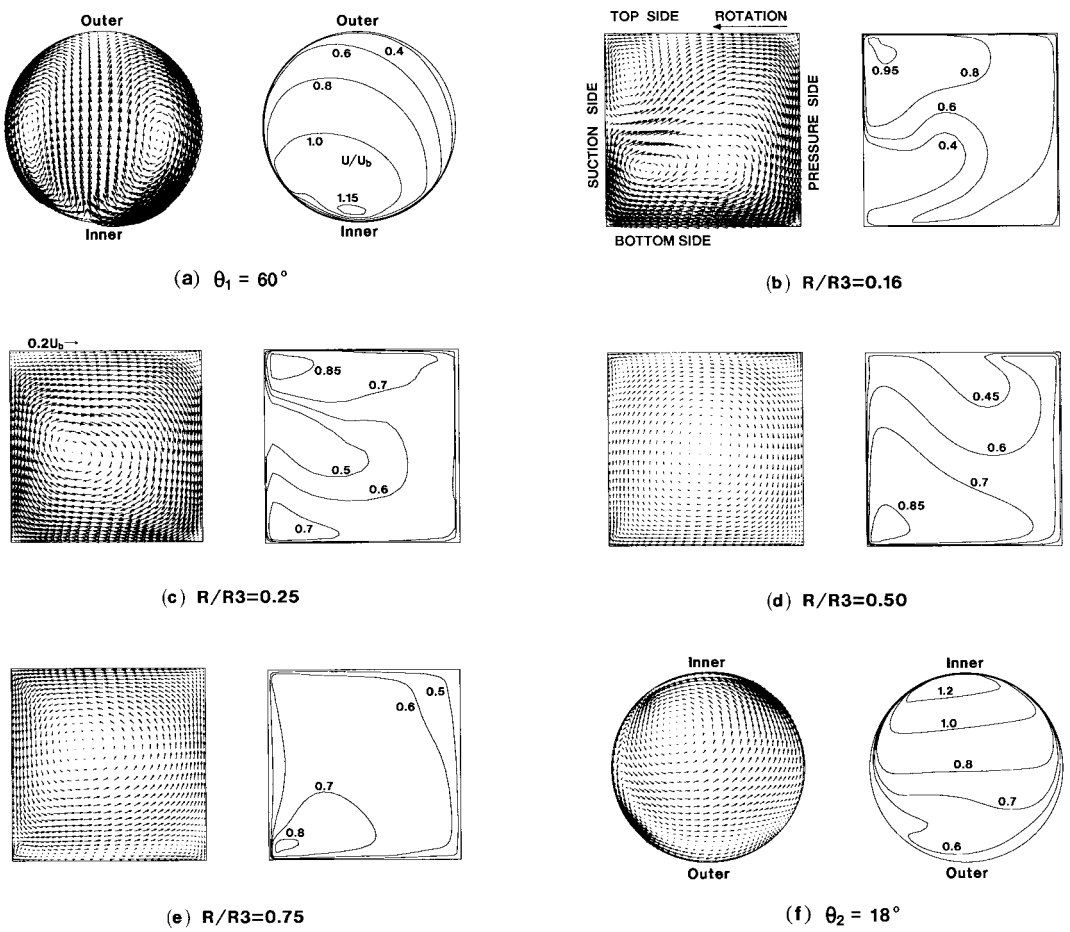

Figure 3. Predicted secondary flow velocity and streamwise velocity contours for $\alpha_0 = 0$.

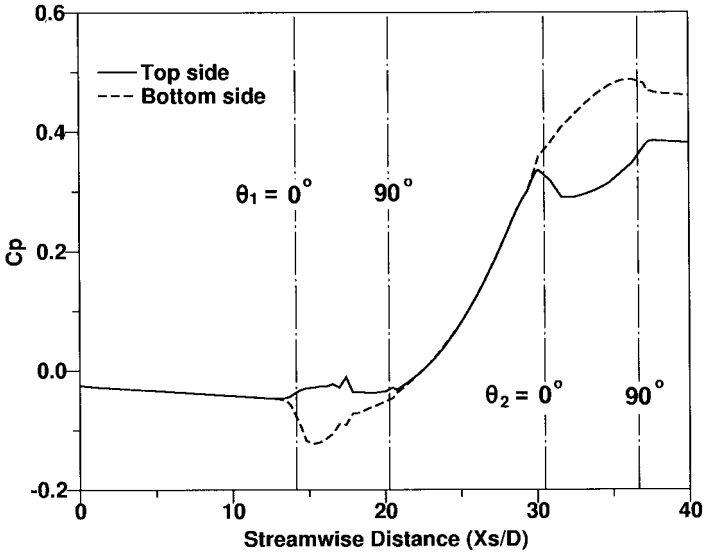

Figure 4. Streamwise wall pressures along vertical symmetry plane for $\alpha_0 = 0$.

a pressure-driven secondary motion convects the fast moving fluid towards the inner wall with an inclination to the rotational direction, causing a substantial deformation of the streamwise velocity contours. As the fluid flows through the square-sectioned straight duct, the Coriolis force is primarily responsible for the generation of the secondary flow. However, due to the effect of the first bend, the secondary flow asymmetric with two large dominant vortices generates upstream of the straight duct (Figure 3(b)). It evolves into an asymmetric multieddy structure dominated by a large vortex with a gradual reduction of the strength downstream of the straight duct, as can be seen from Figure 3(c)–(e). As a result of the secondary motion, the streamwise velocity contours are seen to be further deformed with the displacement of the fast moving fluid from the corner of top and suction sides (Figure 3(b)) toward the corner of bottom and suction sides (Figure 3(c)–(e)). Such a flow pattern is completely different from that predicted for the sole rotating square sectioned duct, where the secondary flows develop a structure with one or two pair of symmetric eddies, depending on the Rossby number; while the fast moving fluid symmetrically occupies the pressure side [8]. This indicates the significant effect of the inlet condition on the developing flow. As the fluid flows through the second bend, it presents a similar effect on the secondary and streamwise velocities to the first bend as can be noted from Figure 3(f).

In Figure 4, the predicted streamwise wall pressure coefficient $C_p = (p - p_{ref})/\rho(\Omega R_3)^2$ (p_{ref} is the average pressure at the cross-section of $R/R_3 = 0.16$) along the vertical symmetry plane is presented. Along the upstream circular pipe, pressure presents a linear reduction. At the two bends, the outer wall pressure is greater than the inner wall pressure, confirming the influence of curvature. As the fluid flows through the square-sectioned duct, the centrifugal force arising from the rotation leads to an accelerated pressure rise along the top and bottom surfaces.

Figure 5 presents a comparison of the predicted pressure coefficient C_p with the experimental data by Minemura *et al.* [6] along the pressure and suction surfaces at the horizontal center plane of the square-sectioned duct. The prediction agrees well with the data, except that the measuring location near the inlet of the straight duct. The severe drop in pressure near the inlet of the straight duct in the measurement is attributable to hydraulic losses through the complex

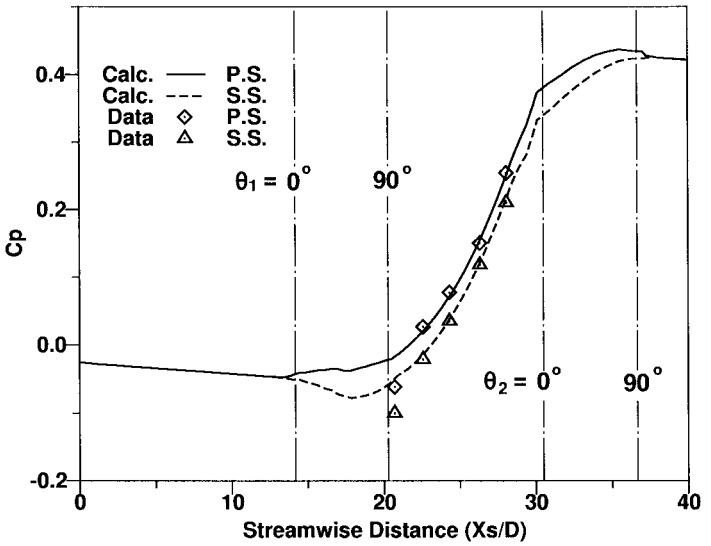

Figure 5. Comparison of predicted and measured pressures along walls of horizontal center plane for $\alpha_0 = 0$.

transition section [6], connecting the bend to the square-sectioned duct, which fails to be exactly represented in the present calculation.

5. RESULTS OF GAS–LIQUID TWO-PHASE FLOW

In Figure 6, the predicted void fraction contours at the projective horizontal center plane are compared with the experimental data by Minemura *et al.* [6]. The prediction shows fair agreement with the data within the whole flow passage. In particular, it reasonably reproduces the accumulation of gas bubbles near the inlet of the straight duct. Such an accumulation had not been captured by the authors previous numerical computations conducted for the sole square-sectioned duct without inclusion of the two bends in the computational domain [8,9].

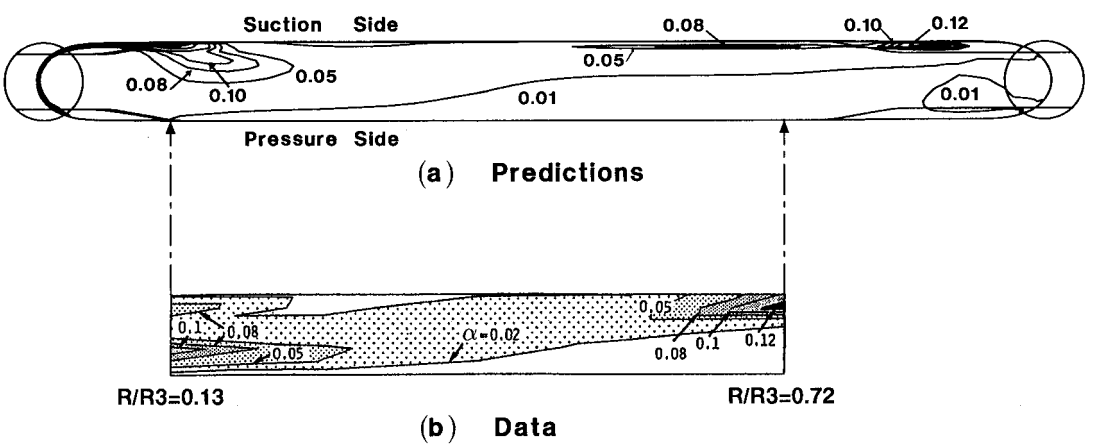

Figure 6. Comparison of predicted and measured void fractions at horizontal center plane.

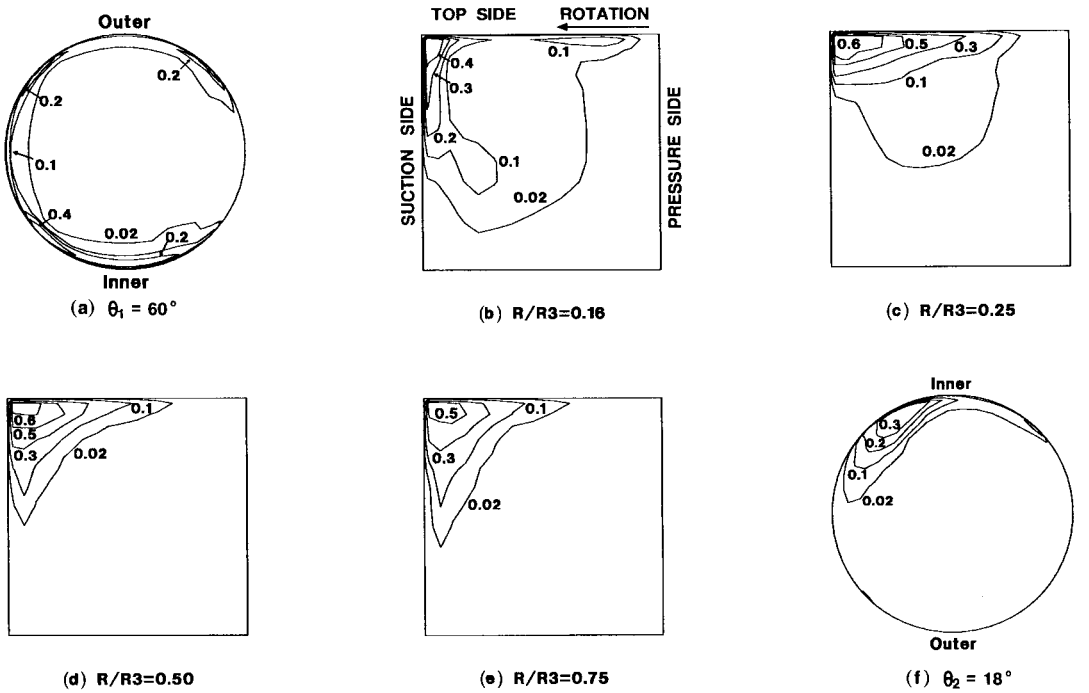

Figure 7. Predicted void fraction contours at different cross-sections.

On the other hand, the previous computations also considerably overpredicted the void fractions over most of the flow passage. This suggests again that the inlet condition has a substantial effect on the void fraction distributions for the developing turbulent two-phase flows.

The predicted void fraction contours at different cross-sections of the duct are displayed in Figure 7. Within the whole flow passage of the duct, the void fractions are seen to present a remarkably non-uniform distribution. At the cross-section of $\theta_1 = 60°$ shown in Figure 7(a), a predominant zone of higher void fractions appears near the inner wall and along the left side wall due to the effects of lateral pressure gradient and the secondary motion. As the bubbles enter the square-sectioned duct, the lateral pressure gradient produced by the Coriolis force drives the gas bubbles to migrate towards the suction side of the duct, and the gravitational buoyancy causes the bubbles to move towards top side of the duct. Consequently, a large number of bubbles accumulate near the corner of the suction and top sides, forming a predominant zone of higher void fractions there, and leaving very few bubbles along the whole pressure and bottom sides, as can be seen from Figure 7(b)–(e). At the station of $\theta_2 = 18°$ shown in Figure 7(f), the predominant zone of higher void fractions occupies the inner wall due to the influence of curvature and the secondary motion.

The predicted secondary velocity vectors and the corresponding streamwise velocity contours for liquid-phase at different cross-sections are illustrated in Figure 8. The secondary flow presents similar patterns to those of single-phase flow, but with some differences of the strength and positions of the vortices, as can be seen from Figure 8(a)–(d). From the inlet region ($R/R_3 = 0.16$) to the middle ($R/R_3 = 0.5$) of the straight duct, the predicted liquid-phase streamwise velocities display similar distributions to those of single-phase flow, but with a

lower maximum value and slight shift of the maximum velocities to the pressure and bottom sides, as shown in Figure 8(a)–(c). Downstream to the outlet of the duct, however, the streamwise velocity contours are different from their counterparts in single-phase flow. The maximum streamwise velocity is further displaced to the pressure side as can be noted from Figure 8(d). As already predicted in previous studies [8,9], it is interesting to note again that a small recirculation zone appears at the corner of top and suction sides and extends downstream of the straight duct, due to the predominant zone of higher void fractions there and the effects of the adverse pressure gradient created by the centrifugal force.

Figure 9 shows the comparison of the predicted turbulence kinetic energy between the single-phase (left) and two-phase flows (right). In the upstream region of the duct, the maximum kinetic energy in two-phase flow is much smaller than that predicted in single-phase flow, as can be seen from Figure 9(a) and (b). Downstream to the outlet of the straight duct, however, the predictions present a reverse, i.e. the maximum kinetic energy in two-phase flow is much greater than its counterpart in single-phase flow, as can be observed from Figure 9(c) and (d). It is interesting to note that the maximum kinetic energy in two-phase flow tends to occupy the region where a predominant zone of higher void fractions exists.

The streamwise wall pressure coefficient C_p along the vertical symmetry plane is predicted for the two-phase flow as shown in Figure 10. In comparison with the single-phase flow (Figure 4), the outer wall pressure is seen to drop severely at the first bend and to increase slightly at the second bend, due to the effect of the gravitational buoyancy. The bottom wall pressure is larger than the top wall pressure along the square-sectioned duct for the same effect of the gravitational buoyancy.

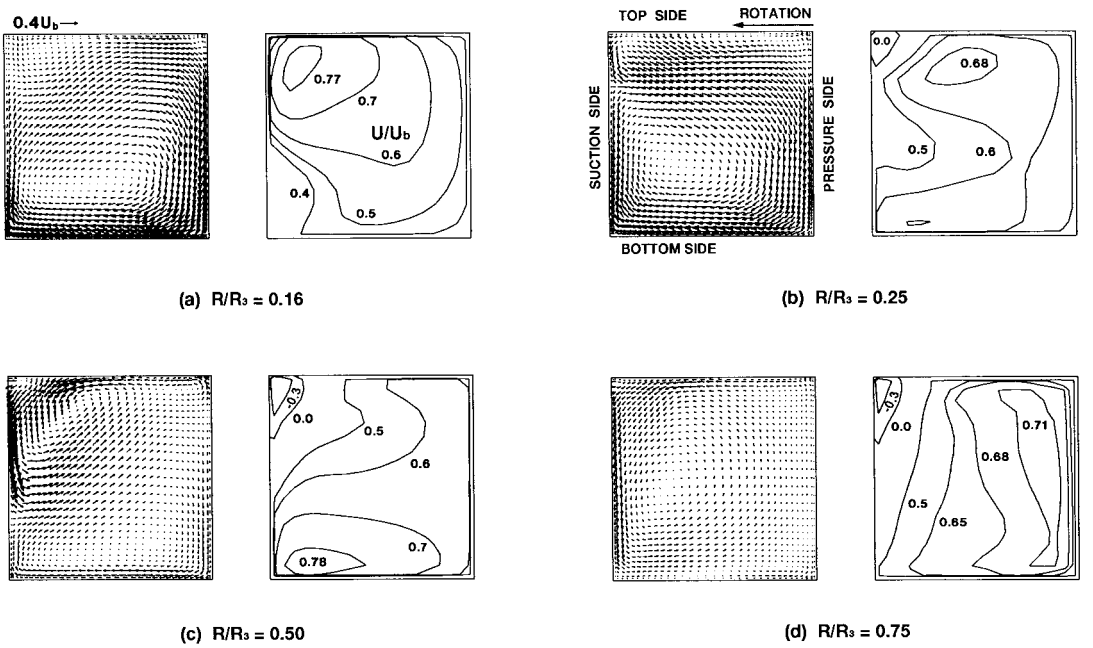

Figure 8. Predicted secondary flow velocity and streamwise velocity contours for liquid-phase at different cross-sections for $\alpha_0 = 0.032$.

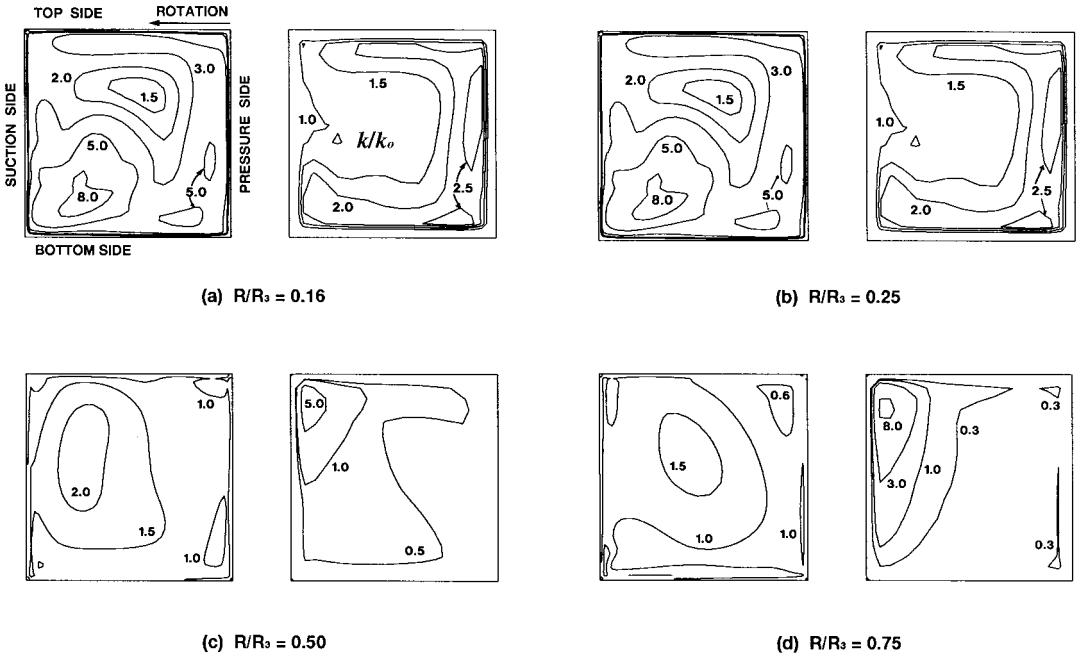

Figure 9. Comparison of predicted turbulence kinetic energy between single-phase and two-phase flows.

The predicted pressure coefficient C_p along the pressure and suction surfaces at the horizontal center plane is compared with the experimental date [6] in Figure 11. The prediction shows good agreement with the data, except the first pair of measuring points near the inlet of the straight duct for the early discussed reasons.

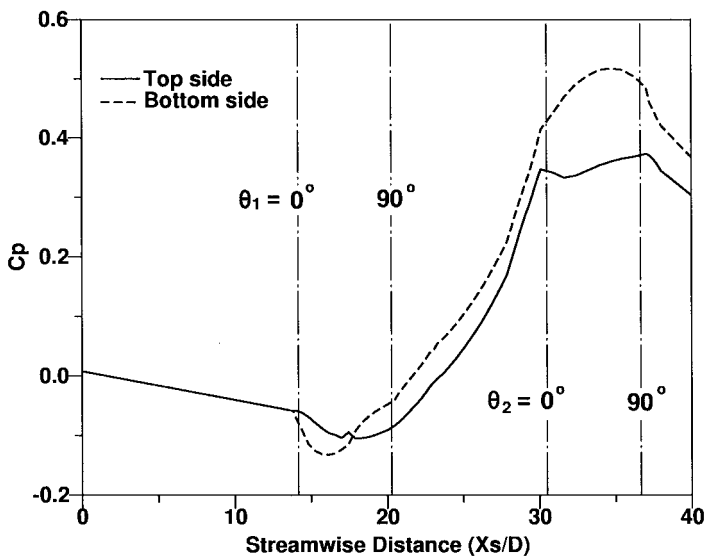

Figure 10. Streamwise wall pressures along vertical symmetry plane for $\alpha_0 = 0.032$.

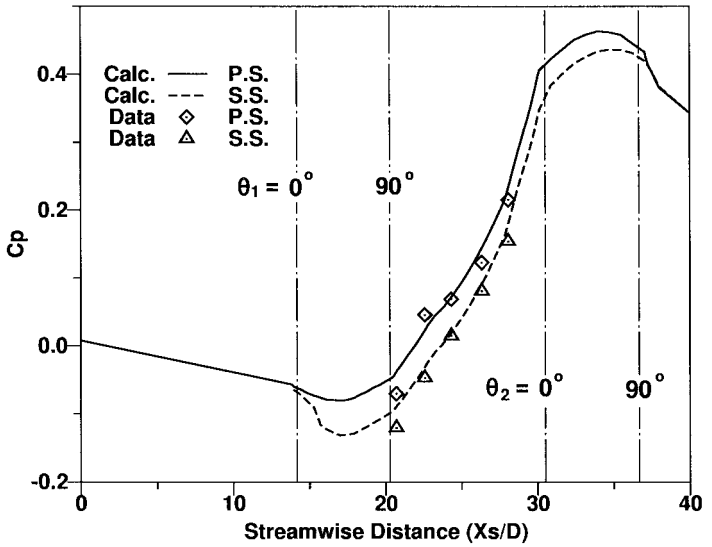

Figure 11. Comparison of predicted and measured pressures along walls of horizontal center plane for $\alpha_0 = 0.032$.

6. CONCLUSIONS

A fully three-dimensional approach, based on the two-fluid model in a general curvilinear co-ordinate system, has been presented and applied to the developing turbulent bubbly two-phase flow in a rotating complicated duct. The main findings of the present study are summarized as follows:

(1) For the single-phase flow, the predictions indicate that the secondary flows are evolved from two large asymmetric dominant vortices into an asymmetric multieddy structure, dominated by a large vortex with a gradual reduction of the strength downstream of the square-sectioned duct. The streamwise velocity contours are strongly deformed by the secondary motion with the displacement of the fast moving fluid towards the corner of bottom and suction sides downstream of the square-sectioned duct.

(2) For the two-phase flow, the predicted void fractions at the horizontal centerplane of the square-sectioned duct show satisfactory agreement with the measurements.

(3) Owing to the effects of rotation, gravity and curvature of the bends, the void fraction distributions present a remarkable non-uniformity within the duct, with the predominant zone of higher void fractions appearing near the top and suction walls of the square-sectioned duct and occupying the inner walls of the two bends.

(4) The predicted pressures agree well with the experimental data for both of the single- and two-phase flows.

REFERENCES

1. K. Minemura and T. Uchiyama, 'Three-dimensional calculation of air–water two-phase flow in centrifugal pump impeller based on a bubbly flow model', *ASME J. Fluids Eng.*, **115**, 766–771 (1993).
2. K. Minemura and M. Murakami, 'Distributions of velocity and void fractions in a radial flow pump impeller handling air–water two-phase mixtures', *Proc. Cavitation and Multiphase Flow Forum*, ASME, Atlanta, USA, 1986, pp. 35–38.
3. A.P. Clarke and R.I. Issa, 'Numerical prediction of bubble flow in a centrifugal pump', *Advances in Multiphase Flow*, Elsevier, Amsterdam, 1985, pp. 175–181.

4. A.D. Gosman, C. Lekakou, S. Politis, R. I. Issa and M.K. Looney, 'Multidimensional modeling of turbulent two-phase flows in stirred vessels', *AIChE J.*, **38**, 1946–1956 (1992).
5. B.R. Patel and P.W. Runstadler, 'Investigations into the two-phase flow behavior of centrifugal pumps', *Proc. of Polyphase Flow in Turbomachinery*, *ASME*, 1978, pp. 79–100.
6. K. Millemura, T. Uchiyama and T. Ishikawa, 'Experimental investigations on bubbly flows in a straight channel rotated around an axis perpendicular to the channel', *Int. J. Multiphase Flow*, **19**, 439–450 (1993).
7. T. Uchiyama, K. Minemura and T. Emura, 'Numerical simulation of bubbly flows in a rotating straight channel using Reynolds stress based on mixing length theory (in Japanese)', *Trans. Jpn. Soc. Mech. Eng.*, **60B**, 2967–2975 (1994).
8. K. Minemura, J-C. Wu and T. Uchiyama, 'Numerical prediction of developing turbulent bubbly flow in a rotating square-sectioned duct (in Japanese)', *Trans. Jpn. Soc. Mech. Eng.*, **62B**, 3784–3791 (1996).
9. J.-C. Wu and K Minemura, 'Effects of turbulence on the phase distribution for developing two-phase flow in a rotating square-sectioned duct', *Proc. JSME Centennial Congress*, *Int. Conf. on Fluid Eng.*, Tokyo, 1997, pp. 473–478.
10. S.J. Lee, R.T. Lahey and O.C. Jones, 'The prediction of two-phase turbulence and phase distribution using a k–ϵ model', *Jpn. J. Multiphase Flow*, **3**, 335–368 (1989).
11. M. Lopez de Bertodano, S.J. Lee, R.T. Lahey and D.A. Drew, 'The prediction of two-phase turbulence and phase distribution phenomena using a Reynolds stress model', *ASME J. Fluids Eng.*, **112**, 107–113 (1990).
12. M. Lopez de Bertodano, R.T. Lahey and O.C. Jones, 'Phase distribution in bubbly two-phase flow in vertical ducts', *Int. J. Multiphase Flow*, **20**, 805–818 (1994).
13. M. Lopez de Bertodano, R.T. Lahey and O.C. Jones, 'Development of a k–ϵ model for bubbly two-phase flow', *ASME J. Fluids Eng.*, **116**, 128–134 (1994).
14. J.H.G. Howard, S.V. Patankar and R.M. Bordynuik, 'Flow prediction in rotating ducts using Coriolis-modified turbulence models', *ASME J. Fluids Eng.*, **102**, 456–461 (1980).
15. C.M. Rhie and W.L. Chow, 'Numerical study of the turbulent flow past an airfoil with trailing edge separation', *AIAA J.*, **21**, 1525–1532 (1983).
16. S. Majumdar, 'Role of underrelaxation in momentum interpolation for calculation of flow with non-staggered grids', *Numer. Heat Transf.*, **13**, 125–132 (1988).
17. D.B. Spalding, 'Mathematical methods in nuclear-reactor thermal hydraulics', *Proc. of American Nuclear Reactor Thermal Hydraulics*, Saratogu, New York, 1980.
18. M. Ishii and N. Zuber, 'Drag coefficient and relative velocity in bubbly droplet or particulate flows', *AIChE J.*, **25**, 843–854 (1979).
19. D.A. Drew and R.T. Lahey Jr., 'The virtual mass and lift force on a sphere in rotating and inviscid flow', *Int. J. Multiphase Flow*, **13**, 113–121 (1987).
20. M. Lance and J. Bataille, 'Turbulence in the liquid phase of a unifrom bubbly air–water flow', *J. Fluid Mech.*, **22**, 95–118 (1991).
21. A. Serizawa, I. Kataoka and I. Michiyoshi, 'Turbulent structure of air–water flow', *Int. J. Multiphase Flow*, **2**, 235–246 (1975).
22. K. Ohba and T. Yuhara, 'Study on vertical bubbly flow using laser doppler measurement (in Japanese)', *Trans. Jpn. Soc. Mech. Eng.*, **48B**, 78–85 (1982).
23. R.I. Issa and P.J. Oliveira, 'Numerical prediction of phase separation in two-phase flow through T-junctions', *Comput. Fluids*, **23**, 347–372 (1994).
24. S.K. Wang, S.J. Lee, O.C. Jones Jr. and R.T. Lahey, '3D turbulence structure and phase distribution measurements in bubbly two-phase flows', *Int. J. Multiphase Flow*, **13**, 327–343 (1987).
25. W. Shyy, S. Thakur and J. Wright, 'Second-order upwind and central difference schemes for recirculating flow computation', *AIAA J.*, **30**, 923–932 (1992).
26. M. Peric, 'A finite volume method for the prediction of three-dimensional fluid flow in complex ducts', *Ph.D. Thesis*, Mechanical Engineering Department, Imperial College, London, 1985.
27. J.L. Marie, 'Modelling of the skin friction and heat transfer in turbulent two-component bubbly flows in pipes', *Int. J. Multiphase Flow*, **13**, 309–325 (1987).
28. N. Zuber and A. Findley, 'Average volumetric concentration in two-phase flow system', *ASME J. Heat Transf.*, **87**, 453–468 (1965).
29. J.C. Wu, K. Minemura and W. Fukatsu, 'Numerical prediction of developing turbulent flow in a curved rotating pipe', *Proc. 5th Asian International Conference on Fluid Machinery*, Seoul, South Korea, 1987, pp. 639–646.

